Received: Added at production | Revised: Added at production | Accepted: Added at production

DOI: xxx/xxxx

SPECIAL ISSUE PAPER

MPM-driven Dynamic Desiccation Cracking and Curling in Unsaturated Soils

Zaili Tu[1] | Chen Peng[1] | Chen Li[1] | Chenhui Wang[1] | Long Liu[1] | Changbo Wang[1] | Hong Qin[2]

[1]School of Computer Science and Technology, East China Normal University, Shanghai, China

[2]Department of Computer Science, Stony Brook University, Stony Brook, New York, USA

Correspondence
Chen Li, School of Computer Science and Technology, East China Normal University, 3663 North Zhongshan Road, Shanghai, China. Email: cli@cs.ecnu.edu.cn

Present Address
This is sample for present address text this is sample for present address text

Abstract

Desiccation cracking of soil-like materials is a common phenomenon in natural dry environment, however, it remains a challenge to model and simulate complicated multi-physical processes inside the porous structure. With the goal of tracking such physical evolution accurately, we propose an MPM based method to simulate volumetric shrinkage and crack during moisture diffusion. At the physical level, we introduce Richards equations to evolve the dynamic moisture field to model evaporation and diffusion in unsaturated soils, with which a elastoplastic model is established to simulate strength changes and volumetric shrinkage via a novel saturation-based hardening strategy during plastic treatment. At the algorithmic level, we develop an MPM-fashion numerical solver for the proposed physical model and achieve stable yet efficient simulation towards delicate deformation and fracture. At the geometric level, we propose a correlating stretching criteria and a saturation-aware extrapolation scheme to extend existing surface reconstruction for MPM, producing visual compelling soil appearance. Finally, we manifest realistic simulation results based on the proposed method with several challenging scenarios, which demonstrates usability and efficiency of our method.

KEYWORDS:
physics-based simulation, soil cracks simulation, material point method, mesh reconstruction

1 | INTRODUCTION

As one of the most common seen and fundamental materials in the natural environment, the modeling and simulation of soil become one of the most important parts in the physics based nature scene simulation. In the computer graphics community, soil is usually considered as an air-water-solid composite of porous-elastoplastic material. The process of soil desiccation can be described as a complicated multi-physics system, involving coupling and interactions among air, water and solids. According to geoscience theories [1,2], the loss of pore water during evaporation raises the negative pressure within soil, which causes volumetric shrinkage and subsequent initiation and propagation of desiccation cracks as it illustrated in Fig. 1. During the process of drying, there are typically two types of fractures (see Fig. 2). One type occurs vertically to the soil surface, leading to the formation of polygonal sections in the soil. While another type occurs in tandem with the formation of shrinkage cracks and is known as "soil curling" or "soil peeling." In this case, a "peeling" crack propagates parallel to the surface, causing the top layer of soil to peel off. To capture the "peeling" crack, the soil moisture content plays a significant role in the deformation evolution of the microscopic pore structure, which dominates macroscopic phenomena such as shrinkage, fracture, and curling.

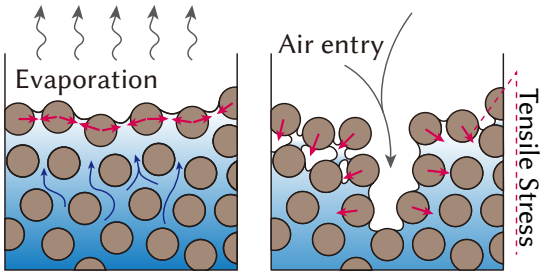

Figure 1 Tensile stress on soil surface increases as evaporation of water, causing soil failure and fracture.

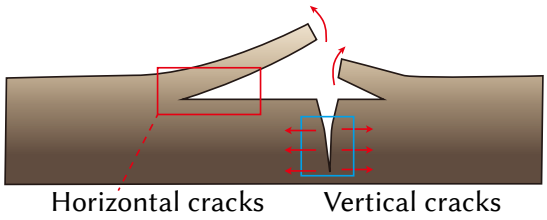

Figure 2 Soil cracking and curling are caused by the formation of vertical and horizontal cracks.

In recent years, MPM has become a proven method for simulating realistic cracking phenomena such as sand-water coupling[3], baking and cooking[4]. However, there still lacks comprehensive exploration on modelling soil-like materials during the moisture movement with MPM for the sake of following challenges.

Firstly, up-to-date fracture simulation methods can not handle horizontal cracks, which frequently occur in multi-layer materials, especially in soils. Secondly, to simulate porous media, most previous methods introduced multi-species theory to model complicated air-water-solid coupling, leading numerical instability and computational inefficiencies. Last but not least, current mesh reconstruction techniques for mesh-free simulation lack of ability to handle cracking surface caused by self-shrinkage.

To overcome the aforementioned challenges, this paper presents a novel approach for simulating the desiccation cracking phenomena for soil-like materials involving shrinkage, curling and fracture. Our contributions are as following:

1. **A saturation-centric elastoplastic model for simulating the dynamic strength and deformation of soil.** We incorporate saturation based pore deformation to track the volumetric changes and hardening states of soil due to pore water movements. As a consequence, our novel model gives prominence to faithful soil phenomena such as desiccation cracking and curling.

2. **An MPM-fashion implicit solver to track pore water movements using Richards equation.** By discretizing Richards equation into MPM, we can evolve the moisture field to effectively handle the pore water movement and evaporation in unsaturated soils, while avoiding time-consuming water-solid coupling in previous techniques.

3. **A surfacing technique that incorporates the moisture to capture visually realistic soil cracking.** We extend previous surfacing techniques for MPM by taking the effects of pore deformation into consideration. By improving the position extrapolation strategy and stretching criteria, our method can preserve more cracking details in soils.

2 | RELATED WORK

Fracture Dynamics

Fracture simulation is a significant research area in the field of computer graphics. FEM was first used to solve large stress problems in brittle and ductile fracture simulations[5,6]. To enhance the level of detail, BEM was introduced by[7] to track boundaries of crack surface. On the other hand, Mesh-free methods such as SPH[8] and MPM[9] have also been proposed. In recent years, Wang et al.[10] successfully captures ductile fracture using MPM and provides a practical way to visualize fracture surface. Further,

combining phase-field-based fracture with MPM [11,12] has shown significant advantages in visualizing the crack surface, Fan et al. [13] further extends this strategy to brittle fracture in MPM.

Surface Tracking Techniques

Surface tracking, i.e, surface reconstruction has been a challenging problem, particularly for objects with frequent changes in topology such as fluids. Osher et al. [14] first applies level-set method for surface tracking, which later be further improved with the inclusion of particles to achieve high-resolution results as proposed by Enright et al. [15]. Brochu et al. [16] developed a framework for robust topological operations on explicit surface meshes, which was further extended to tracking the evolution of multi-material interfaces [17]. Müller et al. [18] employed an Eulerian velocity field to advect the mesh. Wojtan et al. [19] relied on conventional isosurface creation method to generate local meshes when merging and splitting of surface occur. As a post-processing based reconstruction method, Wang et al. [10] tracked surface per-frame instead of per-time-step to gain high performance.

Material Point Method

MPM is considered as a generalization of hybrid methods, such as FLIP [20], to capture both fluid and solid dynamics. MPM was first introduced into computer graphics by [9] to simulate snow. Due to its excellent physical accuracy and natural support for topology changes, MPM has been extensively applied to simulate various phenomena including sand [21], lava [22], viscoelastic/viscoplastic foam [23,24], cloth [25], fracture [10,26,11], magnetized material [27], multi-species coupling [28,4,3], even hydrophobicity and hydrophilicity [29]. In order to address the significant numerical dissipation in MPM, affine particle-in-cell (APIC) [30] incorporated a local velocity gradient to preserve the momentum of particles, and Fei et al. [31] further improved it with several advection strategies.

3 | GOVERNING EQUATIONS

Towards modeling such phenomena, we follow traditional MPM techniques where continuous material is a set of material points carrying certain masses. Motions of these material points are tracked by $\phi : \Omega_0 \times [0,T] \rightarrow \mathbb{R}^3$, where Ω_t denotes the configuration at time t. Motions at time t is defined as $\mathbf{x} = \phi(\mathbf{X}, t)$, and its gradient as $\mathbf{F} = \frac{\partial \phi}{\partial \mathbf{X}}$. We further assume that each particle can be treated as a soil solid with its internal pore water, and air is ignored. Therefore, we have $m = m_s + m_w$, $V = V_s + V_w$, $\rho = m/V$, where the quantities with subscripts s and w represent the amounts of soil and water, and m, V, ρ denote the particle mass, volume, and density, respectively. Here ρ_s, ρ_w are considered as constants, and their ratio affects the overall density.

Compared with current MPM techniques which model interactions of porous water and soil particles as intricacies, we propose a rather concise pipeline under the assumption that contributions of internal moisture movements to the kinematics of soil points can be negligible, based on which the mass and momentum conservation equations of water-soil system can be written as:

$$\frac{\mathrm{D}\rho}{\mathrm{D}t} + \rho \nabla \cdot \mathbf{v}_s = 0, \tag{1}$$

$$\rho \frac{\mathrm{D}\mathbf{v}_s}{\mathrm{D}t} = \nabla \cdot \boldsymbol{\sigma}_s + \rho \mathbf{g}, \tag{2}$$

where $\frac{\mathrm{D}(\cdot)}{\mathrm{D}t} = \frac{\partial(\cdot)}{\partial t} + \mathbf{v}_s \cdot \nabla(\cdot)$ denotes the material derivative, and $\mathbf{g}$ denotes the gravity. We introduce Richards equation to describe the movement of porous water content in unsaturated soils, which is written as:

$$\frac{\mathrm{D}\theta}{\mathrm{D}t} = \nabla D(\theta) \nabla \theta, \tag{3}$$

where θ denotes volumetric water content calculated as V_w/V, $D(\theta)$ denotes the soil water diffusivity, which reflects the changes of diffusion rate based on concentration. In practice, D is a constant, since detailed moisture movement is neglected during crack propagation.

We assume that there are no pore structures within completely dry soil and loss of water content causes the pore structures to become closed, vice versa. Therefore, saturation s of porous water content can be calculated as $s = \theta/\eta$, where initial porosity η is set as the maximum value of volumetric water content.

4 | CONSTITUTIVE MODEL

4.1 | Porous Hyperelasticity

Our moisture-aware deformation $\mathbf{F}$ can be defined as a multiplicative decomposition $\mathbf{F} = \mathbf{F}_s^E \mathbf{F}_s^P \mathbf{F}_w$, where $\mathbf{F}_s^E$ and $\mathbf{F}_s^P$ denote the elastic and plastic deformation contributed by solid, $\mathbf{F}_w$ denotes the pore deformation, which represents the changes in pore volume caused by moisture movements.

For solid stress, the variation of Neo-Hookean model[26] which splits elastic potential into deviatoric and volumetric parts is employed as:

$$\begin{aligned} \Psi(\mathbf{F}) &= \Psi_{dev}(\mathbf{F}_s^E) + \Psi_{vol}(\mathbf{F}_s^E), \\ \Psi_{dev} &= \frac{\mu}{2}(J_s^{E,-2/d}\,\mathrm{tr}(\mathbf{b}) - d), \\ \Psi_{vol} &= \frac{\kappa}{2}(\frac{J_s^{E,2} - 1}{2} - \log(J_s^E)), \end{aligned} \tag{4}$$

where d denotes the dimension, μ denotes shear modulus, κ denotes bulk modulus, $\mathbf{b} = \mathbf{F}_s^{E^T}\mathbf{F}_s^E$ is left Cauchy-Green elastic strain tensor, $J_s^E = \det(\mathbf{F}_s^E)$, Ψ_{dev} and Ψ_{vol} are penalty terms for deviatoric and dilational changes, respectively.

The Kirchhoff stress tensor $\boldsymbol{\tau}$ can be calculated as:

$$\begin{aligned} \boldsymbol{\tau} &= \boldsymbol{\tau}_{dev} + \boldsymbol{\tau}_{vol}, \\ \boldsymbol{\tau}_{dev} &= \mu J_s^{E^{-2/d}}\,\mathrm{dev}(\mathbf{b}), \\ \boldsymbol{\tau}_{vol} &= \frac{\kappa}{2}(J_s^{E^2} - 1)\mathbf{I}, \end{aligned} \tag{5}$$

where $\mathrm{dev}(\boldsymbol{\tau}) = \boldsymbol{\tau} - \frac{1}{d}\,\mathrm{tr}(\boldsymbol{\tau})\mathbf{I}$ denotes the deviatoric part of the tensor. This decomposition greatly simplifies the plasticity solver, as detailed in Sec. 4.2.

For water stress, we assume a linear shrinkage during water loss. Benefiting from above decomposition, the volumetric changes can be solved with the pore deformation $\mathbf{F}_w$ given by:

$$\mathbf{F}_w = ((1-\eta)(1-s) + s)^{1/d}\mathbf{I}, \tag{6}$$

where η denotes the maximum of volumetric water content, and s denotes the current saturation. Inspired by[32], we use similar strategy to always compensate the solid elastic deformation $\mathbf{F}_s^E$ to keep the overall $\mathbf{F}$ unchanged when updating the pore deformation $\mathbf{F}_w$. For example, as the pore saturation decreases, the pore deformation shrinks. To compensate for this shrinkage, the solid elastic deformation $\mathbf{F}_s^E$ expands and effectively cancels out the pore shrinks, creating a false compression that is intuitively caused by local negative pressure. As a result, the material points shrink. Eq. (6) enables our method to capture squeezing stress of pore structure in solids caused by local negative pressure.

4.2 | Saturation-based Hardening Plasticity

Plasticity treatment in MPM involves a yield criterion $y(\boldsymbol{\tau})$, where $y \le 0$ defines the legal region of Kirchhoff stress $\boldsymbol{\tau}$. Any stress violating the condition ($y > 0$) should be projected to the yield surface using return mapping techniques. We adopt the non-associative return mapping algorithm used in[26], which enforces volume preservation, and is written as:

$$\mathbf{b}^{n+1} - \mathbf{b}^{tr} = -2\delta\gamma \boldsymbol{G}(\mathbf{b}^{n+1})\mathbf{b}^{n+1}, \tag{7}$$

where $\mathbf{b} = \mathbf{F}_s^{E^T}\mathbf{F}_s^E$ denotes the left Cauchy-Green elastic strain tensor, $\boldsymbol{G} = \mathrm{dev}(\frac{\partial y}{\partial \boldsymbol{\tau}})$ denotes the projection direction, and $\delta\gamma = \Delta t\gamma$ is an unknown value that represents the projection distance. In practice, we first update the deformation $\mathbf{F}_s$ considering only elasticity to obtain $\mathbf{F}_s^{tr}$, and then correct the illegal deformation using return mapping to obtain the final $\mathbf{F}_s^{n+1}$. More implementation details will be discussed in Section 5.1.

To address the realistic soils elastoplasticity, Non-Associated Cam-Clay (NACC) model[26] is widely used to describe soil-like materials as:

$$y(p,q) = q^2(1+2\beta) + M^2(p+\beta p_0)(p-p_0), \tag{8}$$

where $p = -\frac{1}{3}\,\mathrm{tr}(\boldsymbol{\tau}_{vol})$ denotes the pressure, $q = \sqrt{\frac{6-d}{2}}||\boldsymbol{\tau}_{dev}||$ denotes the shearing, M denotes the friction, and β denotes the cohesivity. And p_0 is a yield pressure related to hardening behavior as $p_0 = \kappa \sinh(\xi \max(-\alpha, 0))$, where κ is the bulk modulus, ξ is the hardening factor, and α is an auxiliary parameter for tracking hardening state.

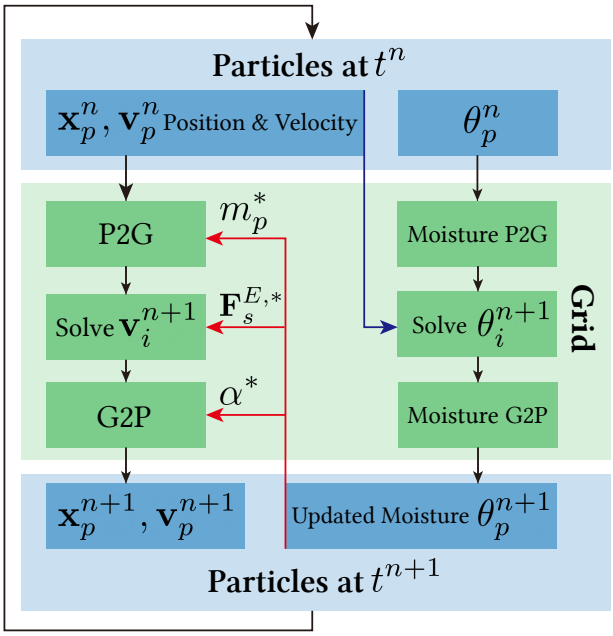

Figure 3 The workflow of our MPM framework, consisting of two solvers staggered coupled with each other.

Based on Eq. (8), we propose a saturation-based hardening strategy for tracking strength changes during desiccation. Specifically, we combine pore deformation to α and track the volumetric shrinkage due to water loss as:

$$\alpha \propto \log(J_s^P J_w), \tag{9}$$

where $J_s^P = \det(\mathbf{F}_s^P)$ and $J_w = \det(\mathbf{F}_w)$, which intuitively connects the moisture loss with hardening process, leading to harder and more brittle behaviors during the shrinkage. We also incorporate the saturation to β as $\beta = \beta_0(1-s) + \beta_1 s$ to model the dynamic cohesivity in consideration of porous water content. ·

5 | DISCRETIZATION AND ALGORITHMIC FLOW FOR SOIL DYNAMICS

Our MPM framework includes two main procedures: solid elastoplastic treatments and moisture evolution. To solve desiccation cracking for soils stably, we discretize proposed dynamic equations to a staggered grid for both solid and moisture steps as detailed in the following paragraphs. For clarity, we denote particle quantities with subscript p, grid node position with subscript i, j and time step with superscript n.

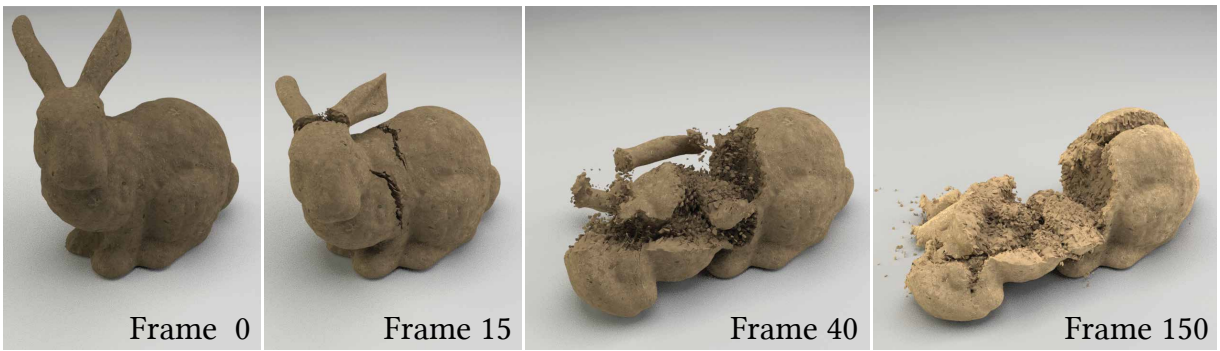

Figure 4 A bunny made with wet soil gradually breaks into a pile of pieces as the water evaporates.

5.1 | Solid Discretization

We discretize governing equations of solid following MLS-MPM[33] as:

Particles to Grid (P2G). We transfer mass and momentum from particles to grid with APIC[30] style: $m_i = \sum_p w_{ip}^n m_p$, $(m\mathbf{v})_i^n = \sum_p w_{ip}^n m_p \left(\mathbf{v}_p^n + \mathbf{C}_p^n(\mathbf{x}_i - \mathbf{x}_p^n)\right)$, where w_{ip}^n is the interpolation weight between node i and particle p at time n, and $\mathbf{C}_p^n$ is the local velocity gradient.

Grid Momentum Update. We calculate forces on grid node as:

$$\mathbf{f}_i^* = -\sum_p V_p^0 M_p^{-1} w_{ip}^n \frac{\partial \Psi}{\partial \mathbf{F}}(\mathbf{F}_{p,s}^n)\mathbf{F}_{p,s}^{n,T}(\mathbf{x}_i - \mathbf{x}_p^n),$$

where $M_p^{-1} = 4/h^2$ is a quadratic interpolation kernel, and V_p^0 is the initial particle volume. Afterwards, we update grid node velocity with $\mathbf{f}_i^n$ as: $\mathbf{v}_i^{n+1} = \mathbf{v}_i^n + \Delta t \frac{\mathbf{f}_i^*}{m_i}$.

Grid to Particles (G2P). We transfer the updated velocities on grids to particles as $\mathbf{v}_p^{n+1} = \sum_p w_{ip}^n \mathbf{v}_i^{n+1}$, also update velocity gradients to $\mathbf{C}_p^{n+1} = \sum_p M_p^{-1} w_{ip}^n \mathbf{v}_i^{n+1}(\mathbf{x}_i - \mathbf{x}_p^n)^T$.

Deformation Gradient Update. We update deformation gradient of particles as: $\mathbf{F}_s^{tr} = (\mathbf{I} + \Delta t \mathbf{C}_p^{n+1})\mathbf{F}_s^n$. Refer to Section 4.2, we apply the plasticity return mapping to obtain final $\mathbf{F}_s^{n+1}$. In detail, there are two types of projections:

- When the volumetric limit is violated ($p^{tr} > p_0$ or $p^{tr} < -\beta p_0$), the final $\mathbf{F}_s^{n+1}$ should ensure that the corresponding stress stays on the nearest tips along the diagonal axis of NACC yield surface.
- When the deviatoric limit is still violated ($y > 0$), we follow the Eq. (7) to obtain the $\mathbf{b}^{n+1}$ then reconstruct $\mathbf{F}_s^{n+1}$. (See supplementary document of[26] for a detailed derivation)

Particles Advection. Finally, we advect particles with updated velocity as: $\mathbf{x}_p^{n+1} = \mathbf{x}_p^n + \Delta t \mathbf{v}_p^{n+1}$.

5.2 | Moisture Discretization

Discretization steps for updating moisture θ_p are proposed as following:

Moisture P2G. We transfer the θ_p from particles to grid: $\theta_i^n = \sum_p w_{ip}^n \theta_p^n$.

Moisture Update. To update moisture, we discretize Eq. (3) in a MPM-fashion, similar to[34], which results in solving a large linear system as:

$$\begin{aligned}
&(\mathbf{M} + \mathbf{L})\boldsymbol{\theta}^{n+1} = \mathbf{M}\boldsymbol{\theta}^n + \mathbf{r},\\
&\mathbf{M} = [m_{ii}] = \sum_p \frac{V_p^n}{\Delta t} w_{ip}^n,\\
&\mathbf{L} = [l_{ij}] = \sum_p V_p^n D \nabla w_{ip}^n \cdot \nabla w_{jp}^n,\\
&\mathbf{r} = [r_i] = \sum_{p \in \partial\Omega^n} S_p^n \lambda(\theta_p^n - \theta_0) w_{ip}^n,
\end{aligned}$$

where $\boldsymbol{\theta}^{n+1}$ is the vector of unknown moisture nodes in the next time step, V_p^n, S_p^n represent volume and area of particle p at time n, θ_0 is the ambient moisture outside. To calculate the contribution of evaporation (introduced in $\mathbf{r}$), we identify boundary grid adjacent to zero-mass grids, and mark all particles within these grids as boundary particles. We use the conjugate gradients (CG) with a Jacobi preconditioner to solve this system, taking the advantage of its high convergence rate for s.p.d. matrices. In practice, the system converges to acceptable residual within 5 iterations.

Moisture G2P. We transfer the updated moisture from grid back to particles as: $\theta_p^{n+1} = \sum_i w_{ip}^n(\theta_i^{n+1} - \theta_i^n)$. To avert numerical noise, we further clamp the water content in between $[0, \eta]$.

Porosity Update. We first evolve saturation and pore deformation with the updated θ_p^{n+1}. Inspired by[32], we make the assumption that the total deformation gradient will not be affected by pore water changes thus causing no plastic deformation, we then update elastic deformation of solid so as to remain $\mathbf{F}_p^n$ be invariant as:

$$\mathbf{F}_{p,s}^{E,*} = \mathbf{F}_p^n(\mathbf{F}_{p,w}^{n+1})^{-1}(\mathbf{F}_{p,s}^P)^{-1}. \tag{10}$$

Meanwhile, we update mass loss and hardening state of each particle according to the saturation-based hardening in Sec. 4.2 as:

$$m_p^* = m_p^n \frac{k_r + s^{n+1}}{k_r + s^n}, \tag{11}$$

$$\alpha_p^* = \alpha_p^n + \epsilon \log \frac{J_w^{n+1}}{J_w^n}, \tag{12}$$

where $k_r = \rho_s/\rho_w$ is a constant ratio during simulation, and ϵ is the hardening rate caused by pore deformation. Finally, our method succeeds in tackling the effects of horizontal soil fracture, i.e., soil peeling and curling. Dataflow of all variables is illustrated in Fig. 3.

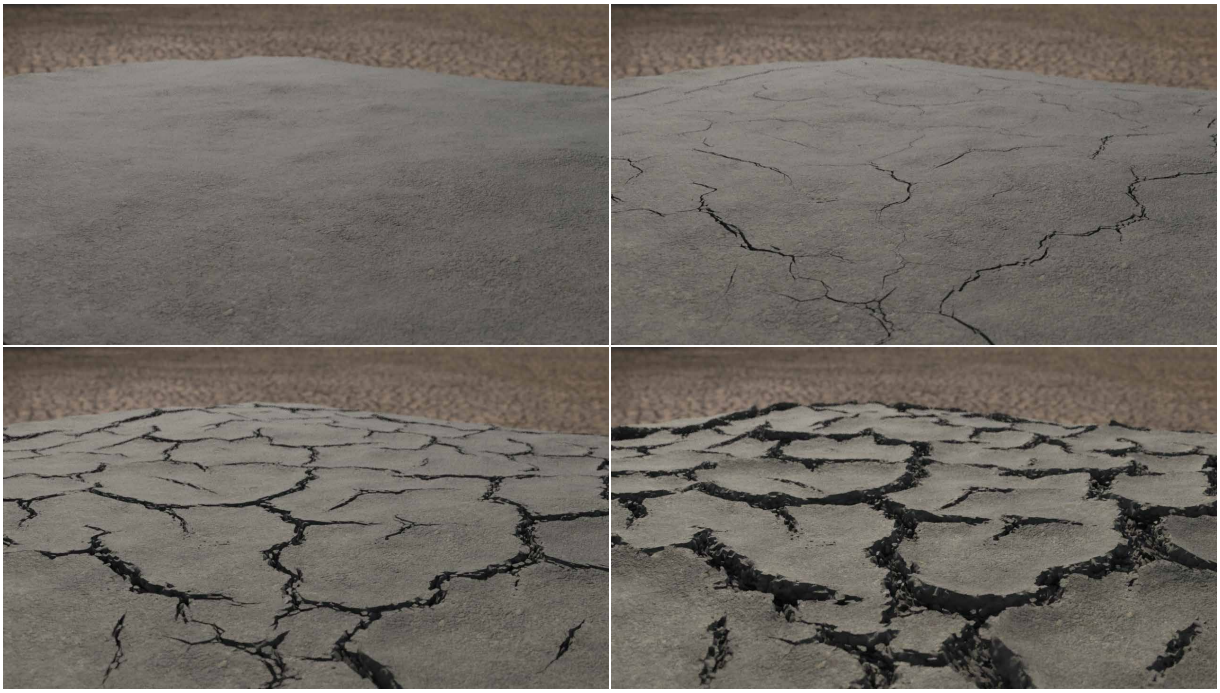

Figure 5 The riverbed dried in the sun appears deep cracks after the ebb tide.

Figure 6 The scale of soil curling varies at different hardening rates.

6 | SURFACE RECONSTRUCTION

Following current MPM mesh reconstruction technique [10], our approach relies on the *particle core* structure, which is constructed by tetrahedralization (triangulation for 2D cases) of MPM particles, to represent surfaces. As proposed by [10], two key factors that dominate mesh reconstruction effects are extrapolation strategy and stretching criteria which influence movement and splitting of particle cores respectively. Towards dedicating surface reconstruction for soil, we additionally introduce the influence of moisture to both factors.

Mesh Extrapolation. We modify the vertices extrapolation strategy in previous technique [10] by introducing $\mathbf{F}_w$ as an extra scaling factor:

$$\mathbf{y}_p^n = \mathbf{F}_w \mathbf{R}(\mathbf{y}_p^0 - \mathbf{x}_p^0) + \mathbf{x}_p^n, \tag{13}$$

where $\mathbf{y}_p^n$ is the core vertex position of MPM particle p, and $\mathbf{R}_p^n$ is the rotation matrix which can be calculated by polar decomposition of $\mathbf{F}_p^n$. Hence, we can accurately track the mesh shrinkage caused by pore water loss, which is ignored in previous works.

Stretching Criteria. For capturing the crack propagation caused by the shrinkage, we replace the constant of stretching criteria with another moisture-correlating scaling factor J_w as:

$$\frac{||\mathbf{x}_p^t - \mathbf{x}_q^t||}{||\mathbf{x}_p^0 - \mathbf{x}_q^0||} > 0.5(J_{p,w} + J_{q,w})\zeta,\ t \leq n, \tag{14}$$

where $J_{p,w}$ and $J_{q,w}$ are determinants of $\mathbf{F}_w$ of particle p and q, ζ is a constant threshold. When Eq. (14) is met, the edge connecting p and q is considered as broken. Benefiting from our adaptive criteria, subtle cracks are more likely to appear on dry soil surface.

Scene	#Particles	Grid Res.	Δt	(ρ_s, E, ν)	NACC$(\alpha_0, \beta, \xi, M)$	Moisture(η, k_r, ϵ)
(Fig. 8)	21K	0.05	1e-3	(1, 2k, 0.35)	(-0.04, 1, 1, 1.87)	(0/0.4, 1, 0/1)
(Fig. 7)	69K	0.03	1e-3	(1, 2K, 0.35)	(0, 0.5, 0.5, 2.43)	(0.5, 1, 0.5)
(Fig. 4)	92K	0.06	1e-3	(2, 1K, 0.35)	(-0.05, 1, 0.5, 2.43)	(0.5, 2, 0.5)
(Fig. 5)	778K	0.2	1e-3	(2, 2K, 0.35)	(-0.05, 1, 0.5, 2.43)	(0.5, 2, 0.6)
(Fig. 6)	230K	0.02	1e-3	(1, 1K, 0.35)	(0, 0.5, 0.5, 2.43)	(0.4, 1, 0.2/0.5/1)
(Fig. 10)	152K	0.06	1e-3	(1, 2K, 0.35)	(0, 0.5, 0.5, 2.43)	(0.5, 1, 0.5)

Table 1 Summary of the simulation settings.

7 | RESULTS

7.1 | Implementation Details

We implement our approach on an AMD Ryzen 7 3700X 8-Core Processor @3.59 GHz CPU, 32G RAM memory, and configurations of our experiments are documented in Tab. 1. To initialize the particles, we generate a high-quality tetrahedral mesh following the approach in [35], then each vertex in the tetrahedral mesh is treated as a MPM particle with full saturation. For better rendering results, our surface reconstruction technique outputs the boundary and crack surface mesh separately, and the UV for suitable texturing is constructed according to the initial mesh.

7.2 | Soil Shrinkage, Crack and Curling

Our proposed method is capable of simulating compelling cracking effects in several challenging scenes, which are described in this subsection. Here we utilize the color intensity as an indicator of the moisture.

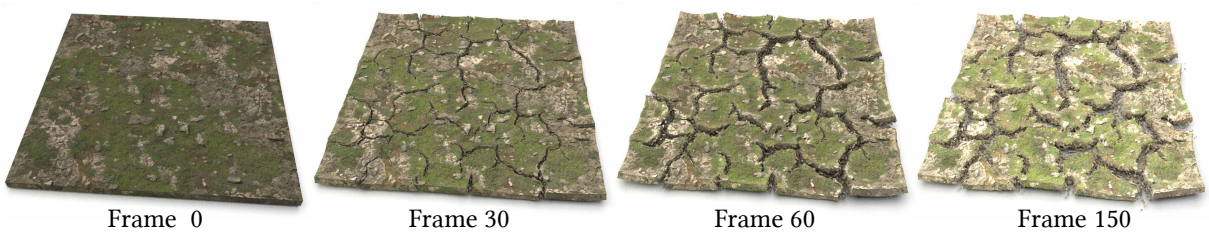

Figure 7 A wet, mossy ground gradually shrinks, cracks and curls as the moisture evaporates.

Fig. 7 shows simulation results of the hardening process. As moisture evaporates with time passes by, the wet and mossy ground simulated with our method appears to shrink, crack and curl as soil in nature will do. We further demonstrate that our method supports simulating soil of complex shapes as depicted in Fig. 4, and can work in conjunction with traditional softening-based fracture. In Fig. 5 we employ our method for a riverbed to further verify the robustness and efficiency of our framework in simulating large-scale terrain.

Fig. 6 shows the simulation results with various hardening rates ϵ. Soil with a larger ϵ tends to be curled more apparently and breach into larger fragments, vice versa.

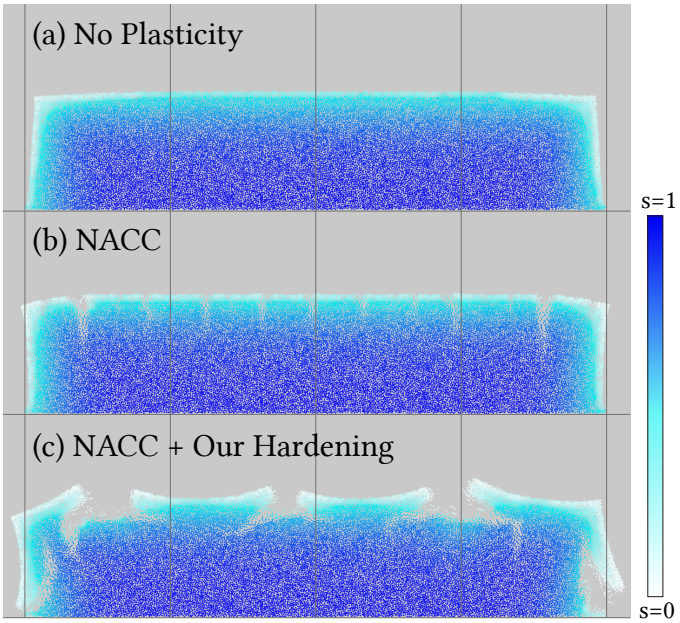

Figure 8 Desiccation experiments under different elastoplastic treatments.

7.3 | Evaluations

To demonstrate the effectiveness of our method, we manifest results simulated with different combination strategies proposed in this paper, including porosity-based shrinkage, NACC with or without our saturation-based hardening. Results in Fig. 8 show effects of our porous term which solves the volumetric shrinkage of soil and produces a rather compacted state. Moreover, Fig. 8(b) and (c) showcase the effects of our saturation-based hardening strategy. In comparison to results simulated with NACC merely (depicted in Fig. 8(b)), where only vertical cracking appears, results using our saturation-based hardening strategy succeeds in simulating surface curling caused by horizontal fractures. We visualize the hardening states of particles as colors in Fig. 9 to intuitively show whether the particles are being stretched or compressed. We also compare surface reconstruction results of our

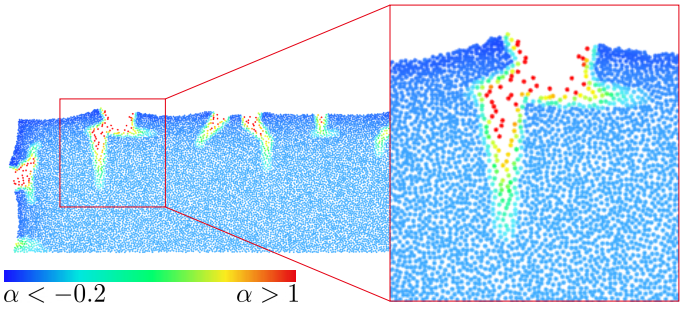

Figure 9 Hardening states during the desiccation.

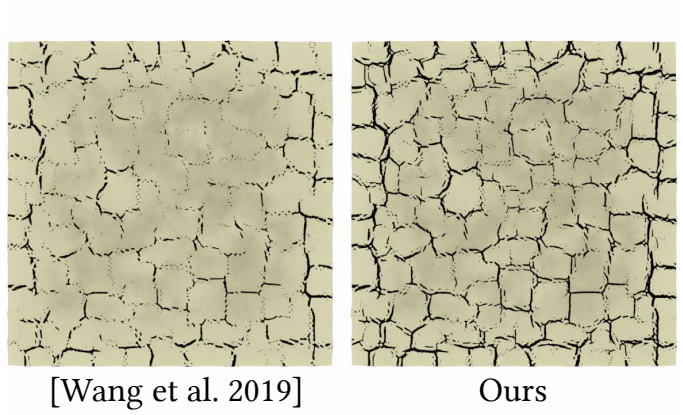

Figure 10 Surface reconstruction results using [10] and our method under the same settings.

saturation-based scheme with previous MPM approach [10]. As shown in Fig. 10, our scheme is able to generate more crackings. What's more, our scheme also accords with the observation that fractures are more likely to appear at dry areas.

7.4 | Limitations

Our approach has certain limitations. Firstly, the presence of sticky numerical artifacts introduced by MPM makes it challenging to generate a clean and sharp internal crack surface. Additionally, due to the lack of geometric definition of cracks during simulation, the local velocity discontinuity caused by cracks cannot be well represented. Furthermore, despite the improved surfacing approach that makes the cracks more prominent, the limitations from the original surfacing technique described in [10] still persist.

8 | CONCLUSION AND FUTURE WORK

In this paper, we presented a novel approach to capture the desiccation cracking of soils, especially vertical and horizontal cracks. We proposed a saturation-centric elastoplastic treatment, in detail, a pore deformation is added to the multiplicative decomposition of deformation gradient to describe the volumetric changes, and a saturation-based hardening strategy is introduced into NACC to enhance the dynamic strength. Also, we developed an MPM-fashion implicit numerical solver to track moisture diffusion and evaporation based on Richards equation, without complicated water-solid coupling handling. For better visual realism, we extended previous surfacing techniques in MPM by introducing the saturation-based scaling factor to reflect the observation that cracks are more likely to appear in dry soil. Based on above technologies, our approach can produce visually compelling results of soil cracks and curls.

In the future, we look forward to apply our method to more porous materials with dynamic moisture by introducing more physical properties and process into our framework. Moreover, it is an exciting direction of investigation to parallelize our method on GPUs to achieve real-time simulations. Finally, our surface reconstruction method is still less ideal, thus its improvement would also be a worthwhile future work.

ACKNOWLEDGEMENTS

This paper is partially supported by Natural Science Foundation of China under Grants 62002121 and 62072183, National Science Foundation of USA (IIS-1715985 and IIS-1812606), Science and Technology Commission of Shanghai Municipality (No.22511104600). The authors would like to express sincere gratitude to these institutions for their support, as well as to all the reviewers for their thoughtful and valuable suggestions.

References

1. Tang C, Zhu C, Cheng Q, others . Desiccation cracking of soils: A review of investigation approaches, underlying mechanisms, and influencing factors. *Earth-Science Reviews* 2021; 216: 103586.

2. Style RW, Peppin SS, Cocks AC. Mud peeling and horizontal crack formation in drying clays. *Journal of Geophysical Research: Earth Surface* 2011; 116(F1).

3. Tampubolon AP, Gast T, Klár G, et al. Multi-Species Simulation of Porous Sand and Water Mixtures. *ACM TOG* 2017; 36(4): 105.

4. Ding M, Han X, Wang S, Gast TF, Teran JM. A Thermomechanical Material Point Method for Baking and Cooking. *ACM TOG* 2019; 38(6): 192.

5. Bao Z, Hong JM, Teran J, Fedkiw R. Fracturing rigid materials. *IEEE TVCG* 2007; 13(2): 370–378.

6. Koschier D, Lipponer S, Bender J. Adaptive Tetrahedral Meshes for Brittle Fracture Simulation. In: Eurographics Association; 2015; Goslar, DEU: 57—66.

7. Glondu L, Marchal M, Dumont G. Real-time simulation of brittle fracture using modal analysis. *IEEE TVCG* 2012; 19(2): 201–209.

8. Chen F, Wang C, Xie B, Qin H. Flexible and rapid animation of brittle fracture using the smoothed particle hydrodynamics formulation. *CAVW* 2013; 24(3-4): 215–224.

9. Stomakhin A, Schroeder C, Chai L, Teran J, Selle A. A Material Point Method for Snow Simulation. *ACM TOG* 2013; 32(4): 102.

10. Wang S, Ding M, Gast TF, et al. Simulation and Visualization of Ductile Fracture with the Material Point Method. *Proc. ACM Comput. Graph. Interact. Tech.* 2019; 2(2): 18.

11. Wolper J, Chen Y, Li M, et al. AnisoMPM: Animating Anisotropic Damage Mechanics. *ACM TOG* 2020; 39(4): 37.

12. Zhao Z, Huang K, Li C, Wang C, Qin H. A Novel Plastic Phase-Field Method for Ductile Fracture with GPU Optimization. *Computer Graphics Forum* 2020; 39(7): 105-117.

13. Fan L, Chitalu FM, Komura T. Simulating Brittle Fracture with Material Points. *ACM TOG* 2022; 41(5): 177:1–177:20.

14. Osher S, Sethian JA. Fronts propagating with curvature-dependent speed: Algorithms based on Hamilton-Jacobi formulations. *Journal of Computational Physics* 1988; 79(1): 12–49.

15. Enright D, Losasso F, Fedkiw R. A fast and accurate semi-Lagrangian particle level set method. *Computers & Structures* 2005; 83(6-7): 479–490.

16. Brochu T, Bridson R. Robust Topological Operations for Dynamic Explicit Surfaces. *SIAM J. Sci. Comput.* 2009; 31(4): 2472–2493.

17. Da F, Batty C, Grinspun E. Multimaterial mesh-based surface tracking. *ACM TOG* 2014; 33(4): 112:1–112:11.

18. Müller M. Fast and robust tracking of fluid surfaces. In: Fellner DW, Spencer SN., eds. *SCA*ACM; 2009: 237–245.

19. Wojtan C, Thürey N, Gross MH, Turk G. Physics-inspired topology changes for thin fluid features. *ACM TOG* 2010; 29(4): 50:1–50:8.

20. Zhu Y, Bridson R. Animating Sand as a Fluid. *ACM TOG* 2005; 24(3): 965–972.

21. Klár G, Gast T, Pradhana A, et al. Drucker-Prager Elastoplasticity for Sand Animation. *ACM TOG* 2016; 35(4): 103.

22. Stomakhin A, Schroeder C, Jiang C, Chai L, Teran J, Selle A. Augmented MPM for Phase-Change and Varied Materials. *ACM TOG* 2014; 33(4): 138.

23. Ram D, Gast T, Jiang C, et al. A Material Point Method for Viscoelastic Fluids, Foams and Sponges. In: Association for Computing Machinery; 2015; New York, NY, USA: 157–163.

24. Yue Y, Smith B, Batty C, Zheng C, Grinspun E. Continuum Foam: A Material Point Method for Shear-Dependent Flows. *ACM TOG* 2015; 34(5): 160.

25. Jiang C, Gast T, Teran J. Anisotropic Elastoplasticity for Cloth, Knit and Hair Frictional Contact. *ACM TOG* 2017; 36(4): 152.

26. Wolper J, Fang Y, Li M, Lu J, Gao M, Jiang C. CD-MPM: Continuum Damage Material Point Methods for Dynamic Fracture Animation. *ACM TOG* 2019; 38(4): 119.

27. Sun Y, Ni X, Zhu B, Wang B, Chen B. A Material Point Method for Nonlinearly Magnetized Materials. *ACM TOG* 2021; 40(6): 205.

28. Fang Y, Qu Z, Li M, et al. IQ-MPM: An Interface Quadrature Material Point Method for Non-Sticky Strongly Two-Way Coupled Nonlinear Solids and Fluids. *ACM TOG* 2020; 39(4): 51.

29. Chen J, Kala V, Marquez-Razon A, Gueidon E, Hyde DAB, Teran J. A momentum-conserving implicit material point method for surface tension with contact angles and spatial gradients. *ACM TOG* 2021; 40(4): 111:1–111:16.

30. Jiang C, Schroeder C, Selle A, Teran J, Stomakhin A. The Affine Particle-in-Cell Method. *ACM TOG* 2015; 34(4): 51.

31. Fei YR, Guo Q, Wu R, Huang L, Gao M. Revisiting Integration in the Material Point Method: A Scheme for Easier Separation and Less Dissipation. *ACM TOG* 2021; 40(4): 109.

32. Chen XS, Li CF, Cao GC, Jiang YT, Hu SM. A Moving Least Square Reproducing Kernel Particle Method for Unified Multiphase Continuum Simulation. *ACM TOG* 2020; 39(6): 176.

33. Hu Y, Fang Y, Ge Z, et al. A Moving Least Squares Material Point Method with Displacement Discontinuity and Two-Way Rigid Body Coupling. *ACM TOG* 2018; 37(4): 150.

34. Gao M, Wang X, Wu K, et al. GPU Optimization of Material Point Methods. *ACM TOG* 2018; 37(6): 254.

35. Hu Y, Schneider T, Wang B, others . Fast Tetrahedral Meshing in the Wild. *ACM TOG* 2020; 39(4): 117.

AUTHOR BIOGRAPHY

Zaili Tu is currently working toward the M.S. degree in School of Computer Science and Technology, East China Normal University, China. He received his B.S. degree in Computer Science and Technology from Zhejiang University of Technology, China, in 2020. His research interest is physics-based animation.

Chen Peng received his BE degree (2016) and PhD degree (2023) in software engineering from School of Software Engineering Institute, East China Normal University, China. His research interests include data-driven animation, physically-based simulation and deep-learning interpretability.

Chen Li is an associate researcher in School of Computer Science and Technology at East China Normal University, P.R. China. He received his Ph.D. degree at the School of Computer Science and Software Engineering, East China Normal University in 2019, and received his BE degree in computer science from Tianjin University in 2013. His research interests include physically based animation, and data-driven approaches with machine learning.

Chenhui Wang received his Bachelor's degree in Computer Science from Hohai University in 2021. He is currently pursuing a Master's degree in Computer Science at East China Normal University, with a research focus on physical based animation and rendering.

Long Liu is currently pursuing a Master's degree at East China Normal University. He previously completed his undergraduate studies at the same university in 2022. His research interests are focused on physics-based animation.

Changbo Wang is a professor of School of Computer Science and Technology, East China Normal University, China. He received his PhD degree at the State Key Lab. of CAD & CG, Zhejiang University in 2006, and received BE degree in 1998 and ME degree in civil engineering in 2002, respectively, both from Wuhan University of Technology. His research interests include physically based modeling and rendering, computer animation and realistic image synthesis, information visualization, and others.

Hong Qin is a Full Professor of Computer Science in Department of Computer Science at State University of New York at Stony Brook (Stony Brook University). He received his BS (1986) degree and his MS degree (1989) in Computer Science from Peking University in Beijing, China. He received his PhD (1995) degree in Computer Science from the University of Toronto. His research interests include Computer Graphics, Geometric and Physics-based Modeling, Computer Aided Design, Computer Aided Geometric Design, Computer Animation and Simulation, Virtual Environments and Virtual Engineering, and others.

How to cite this article: Zaili Tu, Chen Peng, Chen Li, Chenhui Wang, Long Liu, Changbo Wang, and Hong Qin (2023), MPM-driven Dynamic Desiccation Cracking and Curling in Unsaturated Soils, *Comput. Anim. Virtual Worlds*, *2023;00:1–6*.